STRUCTURAL BIOLOGY

Fibril structure of amyloid-β(1–42) by cryo–electron microscopy

Lothar Gremer,[1,2] Daniel Schölzel,[1,2] Carla Schenk,[1] Elke Reinartz,[2] Jörg Labahn,[1,2,3] Raimond B. G. Ravelli,[4] Markus Tusche,[1] Carmen Lopez-Iglesias,[4] Wolfgang Hoyer,[1,2] Henrike Heise,[1,2] Dieter Willbold,[1,2]* Gunnar F. Schröder[1,5]*

Amyloids are implicated in neurodegenerative diseases. Fibrillar aggregates of the amyloid-β protein (Aβ) are the main component of the senile plaques found in brains of Alzheimer's disease patients. We present the structure of an Aβ(1–42) fibril composed of two intertwined protofilaments determined by cryo–electron microscopy (cryo-EM) to 4.0-angstrom resolution, complemented by solid-state nuclear magnetic resonance experiments. The backbone of all 42 residues and nearly all side chains are well resolved in the EM density map, including the entire N terminus, which is part of the cross-β structure resulting in an overall "LS"-shaped topology of individual subunits. The dimer interface protects the hydrophobic C termini from the solvent. The characteristic staggering of the nonplanar subunits results in markedly different fibril ends, termed "groove" and "ridge," leading to different binding pathways on both fibril ends, which has implications for fibril growth.

Amyloids are involved in various diseases, most prominently in many neurodegenerative diseases (*1*–*3*). The amyloid-β protein (Aβ) forms fibrils that further aggregate into plaques that are found in the brains of Alzheimer's disease patients (*4*). These fibrils are structurally highly heterogeneous (*1*, *5*–*8*), which makes the production of highly ordered samples and structure determination difficult. Aβ fibrils have been described as protofilaments intertwined in a helical geometry, existing in several polymorphs, with varying width and helical pitch, different cross-section profiles, and different interactions between the protofilaments (*5*–*7*, *9*, *10*). The local arrangement of Aβ molecules within the fibril can vary drastically between different isomorphs, with potential implications for biological activity (*3*). Data from solid-state nuclear magnetic resonance (NMR) experiments has allowed for building models of Aβ fibrils at atomic resolution (*6*, *7*, *11*–*15*). Here, we present the atomic structure of Aβ(1–42) fibrils by cryo–electron microscopy (cryo-EM) (Figs. 1 and 2 and table S1). To facilitate structure determination, we identified conditions [aqueous solution at low pH containing organic cosolvent; see (*16*)] that yielded a highly homogeneous sample of fibrils as shown by EM and atomic-force microscopy (AFM) [figs. S1 and S2; see (*16*)]. The toxicity of these fibrils was indistinguishable from fibrils grown at neutral pH (fig. S3). Micrographs revealed micrometer-long unbranched fibrils, where about 90% of the fibrils had a rather invariable diameter of about 7 nm (fig. S1). These fibrils were used in a helical reconstruction procedure to compute a three-dimensional (3D) density to 4.0-Å resolution [Figs. 1 and 2 and fig. S4; see (*16*)]. The EM data were augmented by solid-state NMR and x-ray diffraction experiments, which were performed on identically produced fibril samples of recombinant uniformly labeled [^{15}N/^{13}C]-Aβ(1–42) and show that the EM structure is representative of the sample. Full site-specific resonance assignments from 2D and 3D homo- and heteronuclear correlation spectra could be obtained by solid-state NMR for all 42 residues (Fig. 3, A and B; figs. S5 to S7; and tables S2 and S3). For most amino acid residues, only one set of resonances was observed, indicative of high structural homogeneity and order.

The reconstructed fibril density and the atomic model (Fig. 1) show two twisted protofilaments composed of Aβ(1–42) molecules stacked in a parallel, in-register cross-β structure. The separation between the parallel β strands is well visible in the density (Fig. 1A and fig. S8A). The peripheral β sheets (residues 1 to 9 and 11 to 21) are tilted with respect to the fibril axis by ~10° (Fig. 2C). Remarkably, the fibril does not show a C_2 symmetry but instead an approximate 2_1 screw symmetry with a rise of 4.67 Å, which is in excellent agreement with the strongest peak in the x-ray diffraction profile of 4.65 Å (Fig. 3C and fig. S9). Owing to this helical symmetry, the subunits are arranged in a staggered manner (Fig. 4A). The interaction between the protofilaments is thus not true dimeric, but the subunits are stepwise shifted along the fibril axis (fig. S10). Such an arrangement has also been described recently for a dimeric tau fibril structure (*17*).

A single Aβ(1–42) subunit forms an LS-shaped structure, in which the N terminus is L-shaped and the C terminus is S-shaped (Fig. 1D). The C terminus (Fig. 2 and fig. S11, A and B) roughly resembles structures of a different polymorph of Aβ(1–42) determined recently by solid-state NMR (*11*, *13*, *14*) alone (fig. S12 and tables S4 to S6), whereas the dimer interface is completely different (discussed below). In contrast to those NMR structures, the current structure shows the N-terminal part of Aβ(1–42) to be fully visible and part of the cross-β structure of the fibril. Secondary chemical shifts from our NMR experiments and the corresponding secondary structure calculation correlate well with the EM structure

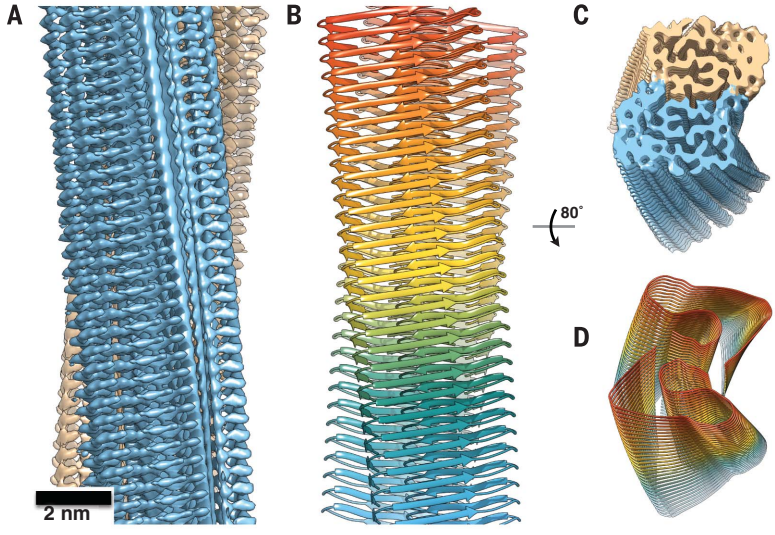

Fig. 1. Aβ(1–42) fibril structure. (**A**) 3D reconstruction from cryo-EM images showing density of two protofilaments (brown and blue) and the clear separation of the β strands. (**B**) Atomic model of the fibril with parallel cross-β structure. (**C** and **D**) Tilted views of the cross section of the EM density and the backbone model.

[1]Institute of Complex Systems, Structural Biochemistry (ICS-6), Forschungszentrum Jülich, 52425 Jülich, Germany. [2]Institut für Physikalische Biologie, Heinrich-Heine-Universität Düsseldorf, 40225 Düsseldorf, Germany. [3]Centre for Structural Systems Biology (CSSB), Deutsches Elektronen-Synchrotron (DESY), 22607 Hamburg, Germany. [4]The Maastricht Multimodal Molecular Imaging Institute, Maastricht University, Universiteitssingel 50, 6229 ER Maastricht, Netherlands. [5]Physics Department, Heinrich-Heine-Universität Düsseldorf, 40225 Düsseldorf, Germany.
*Corresponding author. Email: gu.schroeder@fz-juelich.de (G.F.S.); d.willbold@fz-juelich.de (D.W.)

(Fig. 3B). Although we could not assign the long-range contacts unambiguously, all NMR cross peaks, which are not due to sequential contacts, are in agreement with the cryo-EM structure (figs. S6 and S7). Recently reported chemical shift assignments of two brain seed–derived Aβ(1–42) fibril preparations (*18*) differ from our chemical shifts (table S7), suggesting different polymorphs.

Three hydrophobic clusters stabilize the subunit conformation: (i) Ala[2], Val[36], Phe[4], and Leu[34]; (ii) Leu[17], Ile[31], and Phe[19]; and (iii) Ala[30], Ile[32], Met[35], and Val[40]. Because the hydrophobic clusters expand in the stacked subunits along the fibril axis, they essentially contribute to fibril structure stability (Fig. 4B).

Combined analysis of NMR and cryo-EM data suggests salt bridges between Asp[1] and Lys[28]; Asp[7] and Arg[5]; and Glu[11] and His[6] and His[13] (*16*). The salt bridges of Glu[11] stabilize the kink in the N-terminal part of the β sheet around Tyr[10] (fig. S8D). This structural feature has also been reported for fibrils of the Osaka mutant E22Δ of Aβ(1–40) (*12*). In rat and mouse, which are animal species that are known not to develop Alzheimer's disease, His[13] is replaced by arginine, which possibly prevents the formation of the kink around Tyr[10].

Compared with previous Aβ42 fibril structures (*11*, *13*, *14*), substantial structural differences are observed in the turn region of residues 20 to 25—for example, here only Phe[19], but not Phe[20], is facing the hydrophobic core (Fig. 2 and fig. S12). This region, which forms two of the four edges of the Aβ(1–42) fibril, contains the sites of pathogenic familial mutations of Aβ: Flemish (A21G),

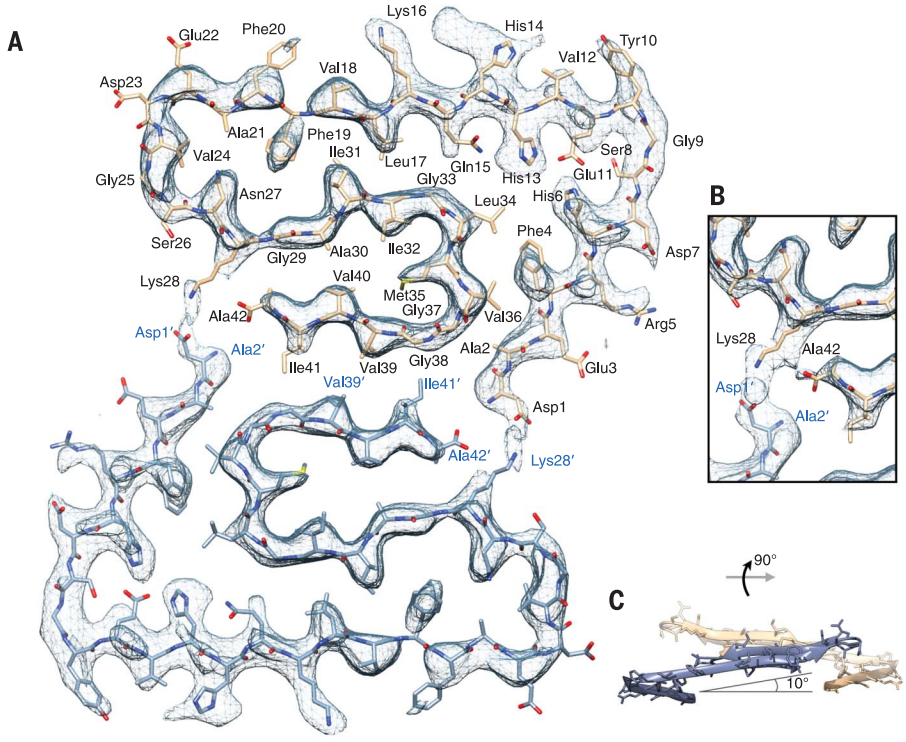

Fig. 2. Atomic model and superimposed EM density of the fibril cross section. (**A**) Two subunits, one from each protofilament, are shown (blue and brown), together with the masked EM density map (at a contour level of 1.5 σ; additional contour levels of 1 σ and 2 σ are shown in fig. S4). (**B**) Detailed view of the interactions between the N and C terminus and the side chain of Lys[28] (at a contour level of 1 σ). (**C**) Side view of the same two opposing subunits showing the relative orientation of the nonplanar subunits. The large peripheral cross-β sheets are tilted by 10° with respect to the plane perpendicular to the fibril axis.

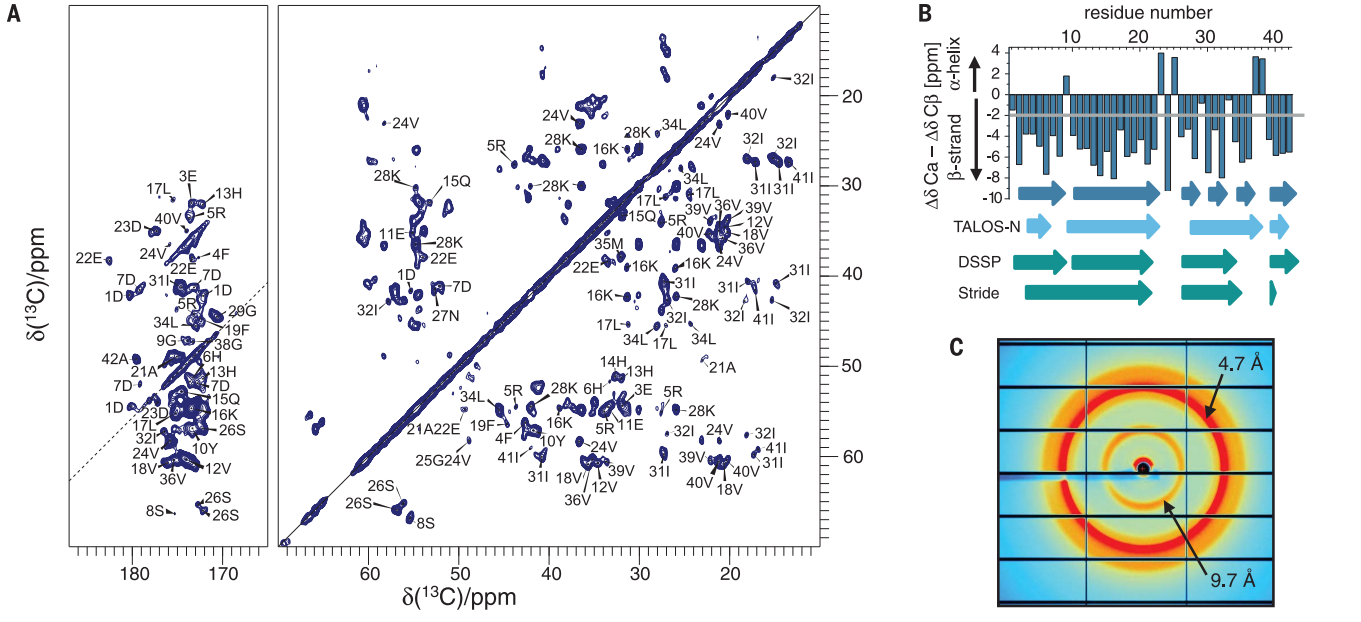

Fig. 3. NMR and x-ray diffraction experiments. (**A**) 2D proton-driven spin diffusion (PDSD) spectrum of fibrillar Aβ(1–42). The spectrum was recorded at a magnetic field strength of 18.8 T, corresponding to a proton Larmor frequency of 800 MHz, a sample temperature of $T = 0 \pm 5$°C, and a spinning speed of 12.5 kHz. For homonuclear $^{13}C/^{13}C$ mixing, PDSD with a mixing time of 20 ms was used. A squared and shifted sine bell function was used for apodization (shift of 0.3·π). (**B**) Secondary chemical shifts calculated from assigned resonance shifts and random coil values predicting β-strand regions [difference exceeds −2 parts per million (ppm)] (dark blue). For Gly residues, only the Cα secondary chemical shifts are plotted. Additionally, β strands calculated by the program TALOS-N and β sheets from the cryo-EM derived atomic model are displayed (assigned by the programs DSSP and Stride). (**C**) X-ray diffraction image of unoriented Aβ(1–42) fibrils. Single-letter abbreviations for the amino acid residues are as follows: A, Ala; C, Cys; D, Asp; E, Glu; F, Phe; G, Gly; H, His; I, Ile; K, Lys; L, Leu; M, Met; N, Asn; P, Pro; Q, Gln; R, Arg; S, Ser; T, Thr; V, Val; W, Trp; and Y, Tyr.

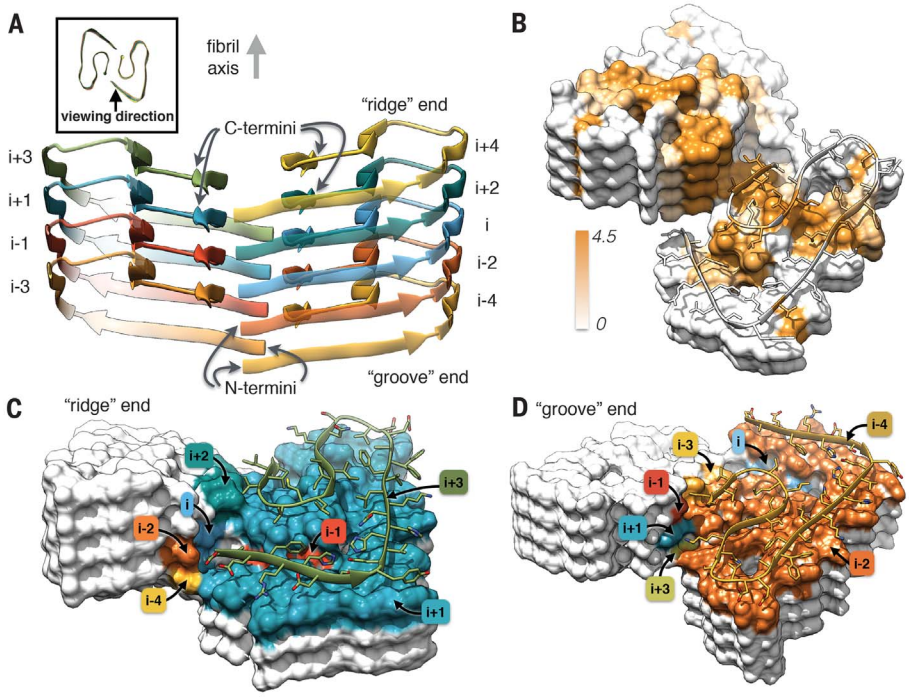

Fig. 4. Details of the Aβ(1–42) fibril architecture. (**A**) Side view of the atomic model showing the staggered arrangement of the nonplanar subunits. (**B**) Surface representation of a fragment of the atomic fibril model. Surface is colored according to hydrophobicity (Kyte-Doolittle scale) [gradient from brown (hydrophobic, 4.5) to white (neutral, 0.0)]. (**C** and **D**) View of the "ridge" (C) and "groove" (D) fibril ends. Only the contact surfaces of the subunits with the respective capping monomer [*i*+3 in (C) and *i*-4 in (D), shown as ribbons] are colored [color coding according to layer number; see (A)].

Arctic (E22G), Dutch (E22Q), Italian (E22K), and Iowa (D23N). Furthermore, the effect of two mutants in the N terminus at Ala[2] can now be rationalized based on the fibril structure: A2T (Icelandic) might be protective against Alzheimer's disease, because threonine is more polar than alanine and could destabilize the fibril by disrupting the hydrophobic cluster Ala[2], Val[36], Phe[4], and Leu[34] (Fig. 2). In contrast, A2V is pathogenic, which could be related to the fact that valine is more hydrophobic than alanine and would strengthen the hydrophobic interaction leading to increased fibril stability.

The staggered arrangement of the subunits has direct implications for fibril growth. Each monomer that binds to a certain fibril end sees the same interface, in contrast to a true dimeric interface (in the case of a C_2 symmetry), where added monomers would alternatingly see either two identical binding sites or a curb preformed by the preceding subunit. The binding sites presented by the two fibril ends are different from each other (Fig. 4, C and D), which leads to different binding pathways with possibly different energy barriers and likely results in polarity of amyloid fibril growth (*19*, *20*). The binding energy, however, has to be identical on both ends. The subunits are not planar; instead, the chain rises along the fibril axis from the N to the C terminus, forming grooves and curbs at the binding interface (Fig. 4, C and D). We refer to the fibril ends as "groove" and "ridge" because β strand 27 to 33 forms a ridge on the surface of one end of the protofilament and a groove on the other end. The β strands are staggered with relation to one another in a zipper-like manner (Fig. 4A and fig. S11C). For example, Phe[4] of subunit *i* is in contact with Leu[34] and Val[36] from the subunit *i*-2 directly below. At both fibril ends, the binding site for the addition of subunit *i* contains contributions of subunits *i*-1, *i*-2, *i*-3, *i*-4, and *i*-5, or *i*+1, *i*+2, *i*+3, *i*+4, and *i*+5, respectively, and very small, likely insignificant contributions from *i*-7 and *i*+7 (fig. S11D). Therefore, five Aβ(1–42) subunits are required to provide the full interface for monomer addition. For a fragment of six subunits, the capping subunits would have the same full contact interface as those in an extended fibril. We define this structural element of six subunits as the minimal fibril unit (fig. S11D).

The protofilament interface is formed by the C termini, in contrast to previously determined solid-state NMR structures (*11*, *13*), where the C termini are solvent-exposed (fig. S12). The interface is hydrophobic in the core and is formed by interactions between residues Val[39] and Ile[41] in subunit *i* with Val[39] and Ile[41] in subunits *i*+1 and *i*-1 (Fig. 4B). Moreover, the N terminus of subunit *i* is close to the C terminus of subunit *i*-3, and the salt bridge between Asp[1] (subunit *i*), and Lys[28] (subunit *i*-5) also stabilizes the interaction between the protofilaments (Figs. 2 and 4). Our structure agrees with a previously reported low-resolution cryo-EM structure of Aβ(1–42) fibrils (*21*), which was prepared under similar low pH conditions, but clearly differs from the polymorph observed in (*9*) (fig. S13A).

Our 4.0-Å structure provides detailed insight into the architecture of Aβ(1–42) amyloid fibrils and reveals a complete model with the backbone of all 42 residues and almost all side chains visible and highly ordered. An in-depth illustration of a protofilament interface is achieved. The regular helical symmetry has direct implications for the mechanism of fibril elongation and results in distinct binding sites for monomeric Aβ, including contacts across different subunit layers. This high-resolution structure will help to understand differences in pathogenic familial mutations and the molecular mechanism underlying fibril growth and potentially will suggest ways to interfere with fibril formation and growth.

REFERENCES AND NOTES

1. R. Riek, D. S. Eisenberg, *Nature* **539**, 227–235 (2016).
2. T. P. Knowles, M. Vendruscolo, C. M. Dobson, *Nat. Rev. Mol. Cell Biol.* **15**, 384–396 (2014).
3. M. Jucker, L. C. Walker, *Nature* **501**, 45–51 (2013).
4. D. J. Selkoe, J. Hardy, *EMBO Mol. Med.* **8**, 595–608 (2016).
5. M. Fändrich, J. Meinhardt, N. Grigorieff, *Prion* **3**, 89–93 (2009).
6. J. X. Lu *et al.*, *Cell* **154**, 1257–1268 (2013).
7. A. K. Paravastu, R. D. Leapman, W. M. Yau, R. Tycko, *Proc. Natl. Acad. Sci. U.S.A.* **105**, 18349–18354 (2008).
8. J. M. Lopez del Amo *et al.*, *Angew. Chem. Int. Ed.* **51**, 6136–6139 (2012).
9. M. Schmidt *et al.*, *Proc. Natl. Acad. Sci. U.S.A.* **112**, 11858–11863 (2015).
10. D. S. Eisenberg, M. R. Sawaya, *Annu. Rev. Biochem.* **86**, 69–95 (2017).
11. M. T. Colvin *et al.*, *J. Am. Chem. Soc.* **138**, 9663–9674 (2016).
12. A. K. Schütz *et al.*, *Angew. Chem. Int. Ed. Engl.* **54**, 331–335 (2015).
13. M. A. Wälti *et al.*, *Proc. Natl. Acad. Sci. U.S.A.* **113**, E4976–E4984 (2016).
14. Y. Xiao *et al.*, *Nat. Struct. Mol. Biol.* **22**, 499–505 (2015).
15. T. Lührs *et al.*, *Proc. Natl. Acad. Sci. U.S.A.* **102**, 17342–17347 (2005).
16. Materials and methods and additional analyses are available as supplementary materials.
17. A. W. P. Fitzpatrick *et al.*, *Nature* **547**, 185–190 (2017).
18. W. Qiang, W. M. Yau, J. X. Lu, J. Collinge, R. Tycko, *Nature* **541**, 217–221 (2017).
19. A. H. DePace, J. S. Weissman, *Nat. Struct. Biol.* **9**, 389–396 (2002).
20. Y. Inoue, A. Kishimoto, J. Hirao, M. Yoshida, H. Taguchi, *J. Biol. Chem.* **276**, 35227–35230 (2001).
21. R. Zhang *et al.*, *Proc. Natl. Acad. Sci. U.S.A.* **106**, 4653–4658 (2009).

ACKNOWLEDGMENTS

The authors gratefully acknowledge the continued support of D. Riesner and G. Büldt. We thank P. J. Peters for advice and helpful discussions, H. Duimel for help with sample preparation, and the M4I Division of Nanoscopy of Maastricht University for microscope access and support. The authors gratefully acknowledge the computing time granted by the Jülich Aachen Research Alliance High-Peformance Computing (JARA-HPC) Vergabegremium and VSR commission on the supercomputer JURECA at Forschungszentrum Jülich. Computational support and infrastructure was provided by the Center for Information and Media Technology (ZIM) at the University of Düsseldorf (Germany). The authors acknowledge access to the Jülich-Düsseldorf Biomolecular NMR Center. D.W. was supported by grants from the Portfolio Technology and Medicine, the Portfolio Drug Design, and the Helmholtz-Validierungsfonds of the Impuls und Vernetzungs-Fonds der Helmholtzgemeinschaft. D.W. is a paid scientific advisor for the Institut de Biologie Structurale (IBS),

CEA, DSV, IBS, 38027 Grenoble (France). H.H. was supported by the Entrepreneur Foundation at the Heinrich-Heine-University of Düsseldorf and by the Deutsche Forschungsgemeinschaft (DFG) (HE 3243/4-1). Support from an European Research Council (ERC) Consolidator Grant (grant agreement no. 726368) to W.H. is acknowledged. The 4.0-Å EM density map of the Aβ(1–42) fibril has been deposited in the Electron Microscopy Data Bank with accession code EMD-3851; the coordinates of the atomic model have been deposited in the Protein Data Bank under accession code 5OQV. The NMR data have been deposited in the Biological Magnetic Resonance Data Bank (BMRB) under accession number 27212. The authors declare no competing financial interests.

SUPPLEMENTARY MATERIALS

www.sciencemag.org/content/358/6359/116/suppl/DC1
Materials and Methods
Figs. S1 to S13
Tables S1 to S7
Movies S1 to S3
References (*22*–*47*)

3 July 2017; accepted 24 August 2017
Published online 7 September 2017
10.1126/science.aao2825

Fibril structure of amyloid-β(1–42) by cryo–electron microscopy

Lothar Gremer, Daniel Schölzel, Carla Schenk, Elke Reinartz, Jörg Labahn, Raimond B. G. Ravelli, Markus Tusche, Carmen Lopez-Iglesias, Wolfgang Hoyer, Henrike Heise, Dieter Willbold and Gunnar F. Schröder

Science **358** (6359), 116-119.
DOI: 10.1126/science.aao2825originally published online September 7, 2017

Elucidating pathological fibril structure

Amyloid-β (Aβ) is a key pathological contributor to Alzheimer's disease. Gremer *et al.* used cryoelectron microscopy data to build a high-quality de novo atomic model of A β fibrils (see the Perspective by Pospich and Raunser). The complete structure reveals all 42 amino acids (including the entire N terminus) and provides a structural basis for understanding the effect of several disease-causing and disease-preventing mutations. The fibril consists of two intertwined protofilaments with an unexpected dimer interface that is different from those proposed previously. The structure has implications for the mechanism of fibril growth and will be an important stepping stone to rational drug design.

Science, this issue p. 116; see also p. 45